Applied Surface Science 412 (2017) 537–544

Contents lists available at ScienceDirect

Applied Surface Science

journal homepage: www.elsevier.com/locate/apsusc

All-solid-state thin film battery based on well-aligned slanted $LiCoO_2$ nanowires fabricated by glancing angle deposition

Miyoung Yoon [a], Seunghwan Lee [b,c], Daehee Lee [a], Joosun Kim [b,*], Jooho Moon [a,*]

[a] Department of Materials Science and Engineering, Yonsei University, Seoul 120-749, Republic of Korea
[b] High Temperature Energy Materials Research Center, Korea Institute of Science and Technology, Seoul 136-791, Republic of Korea
[c] Department of Energy Science, Sungkyunkwan University, Suwon 440-746, Republic of Korea

ARTICLE INFO

Article history:
Received 8 December 2016
Received in revised form 27 March 2017
Accepted 30 March 2017
Available online 2 April 2017

Keywords:
Lithium ion battery
All-solid-state thin film battery
Glancing angle deposition
$LiCoO_2$ nanowire
Electrochemical performance

ABSTRACT

We fabricated all-solid-state thin film batteries based on well-aligned slanted $LiCoO_2$ nanowires by glancing angle deposition, as a facile template-free method in order to increase the electrochemically active site, *i.e.*, the contact area between the solid electrolyte and the electrode. A highly porous thin film composed of well-separated slanted $LiCoO_2$ nanowires not only facilitates the penetration of solid electrolyte phase into the cathode, but also alleviates the thermally and mechanically induced stresses during post-annealing and electrochemical cycling. The all-solid-state thin film battery based on the well-aligned slanted $LiCoO_2$ nanowires, whose contact area between electrolyte and electrode was three times as high as that of a dense thin film, could provide additional migration pathways for lithium ion diffusion due to the enlarged reaction sites. This resulted in enhanced electrochemical kinetics, thereby leading to better rate capability and long-term cyclic stability as compared to the dense $LiCoO_2$ thin film.

1. Introduction

Considerable attention has been directed toward the development of portable, wearable, and implantable lithium ion batteries as future power sources, because of the increasing demand for small electronic devices, such as mobile phones, laptops, and microelectronic biological/medical devices [1–3]. In order to commercialize microelectronic devices, it is necessary that the power sources, *i.e.*, lithium ion batteries, are miniaturized to the micron-size range [3]. However, traditional lithium ion batteries, which consist of liquid electrolytes, are bulky in size and have safety-related issues, including explosion/leakage of highly flammable organic solvents. Therefore, these are incompatible with micro-applications. On the other hand, all-solid-state thin film lithium ion batteries involving solid electrolytes, which excludes the use of hazardous organic solvents, would be suitable for micron-sized batteries with design flexibility [4–6].

Despite their potential, the commercialization of all-solid-state thin film batteries has been impeded by the low electrochemical performance resulting from both the low ionic conductivity of the solid electrolyte and the narrow electrochemically active sites limited to the two-dimensional (2D) planar interface between the solid electrolyte and the electrode [7]. In particular, the cell performance rapidly deteriorated during operation under high current rate conditions above 3 C [8]. Many efforts have been made to develop novel solid electrolytes with high ionic conductivity ($\geq 10^{-2}$ S cm^{-1}) at room temperature, such as $Li_{10}GeP_2S_{12}$ [9,10], Li_3PS_4 [11], and Li_4SnS_4 [12], while the thickness of the solid electrolyte was reduced to below 1 μm to minimize the ohmic loss [13]. However, the sulfide-based electrolytes suffer from poor long-term cyclability [14], and the use of a thinner solid electrolyte does not induce significant improvement of electrochemical performance because of dielectric breakdown associated with thin electrolyte.

As an alternative approach, increasing the electrochemically active site, *i.e.*, the contact area between the solid electrolyte and the electrode, can boost the electrochemical performance of all-solid-state thin film batteries. One-dimensional (1D) nanostructured electrodes can result in increased surface area, and hence, increased contact area between the solid electrolyte and the electrode [15], thereby facilitating the electrochemical reaction kinetics and reducing the distance for lithium ion migration. There are several reports of 1D $LiCoO_2$ nanowire cathode thin films involved in liquid electrolyte-based lithium ion batteries, demonstrating better electrochemical performance than the 2D planar $LiCoO_2$ counterpart [16–18]. However, such 1D nanowire $LiCoO_2$ thin films are yet to be applied to all-solid-state thin film batteries.

Among the numerous available physical and chemical nanostructuring methodologies, solution-based approaches such as the

* Corresponding authors.
E-mail addresses: joosun@kist.re.kr (J. Kim), jmoon@yonsei.ac.kr (J. Moon).

http://dx.doi.org/10.1016/j.apsusc.2017.03.268
0169-4332/

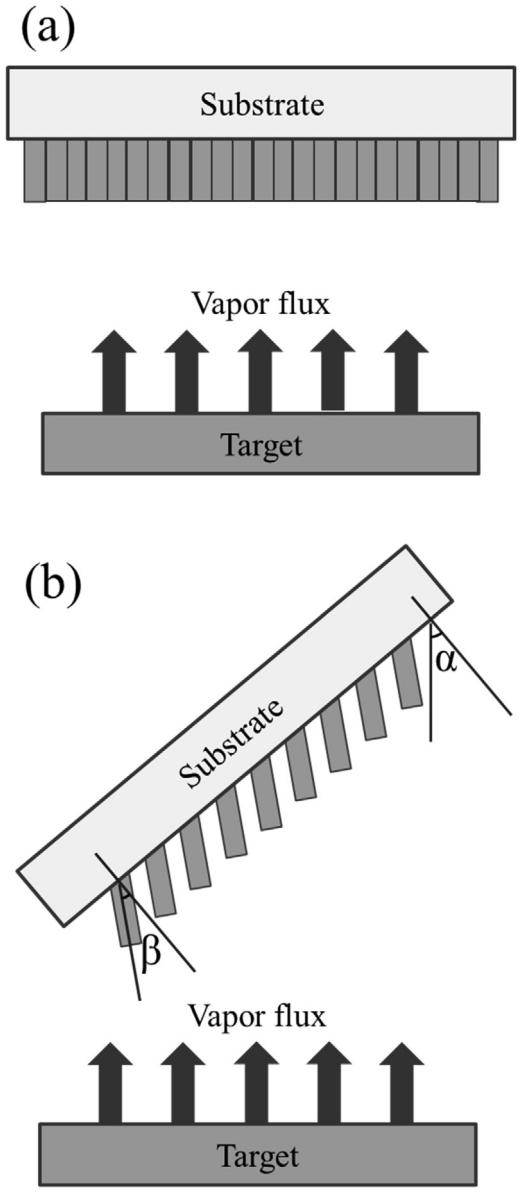

Fig. 1. Schematic diagrams showing the geometrical configurations of the target and substrate in (a) conventional PVD and (b) glancing angle deposition.

template-assisted method or sol-gel process readily enables the fabrication of 1D nanostructured $LiCoO_2$ thin films. However, these methods frequently require additional etching/post-annealing steps. The resulting nanostructures may be poorly dispersed and aligned, making their application to reproducible mass-production of 1D nanostructured $LiCoO_2$ cathodes difficult. As a physical nanostructuring approach, glancing angle deposition (GLAD), which is a physical vapor deposition (PVD) method, constitutes an alternative facile template-free method. In this method, the morphology and alignment of the nanostructures are simultaneously controlled by changing the geometrical configuration of the target and the substrate placed in the deposition apparatus [19–22]. The key feature of GLAD is that the target and the substrate surfaces are not aligned in parallel, unlike the conventional PVD method, but obliquely, as depicted in Fig. 1. During the deposition process, the particles released from the target are obliquely incident to the substrate surface, followed by the formation of separated nuclei with shadowed regions behind them. These shadowed regions cannot receive any more particles, as a result of which the nuclei form well-aligned and

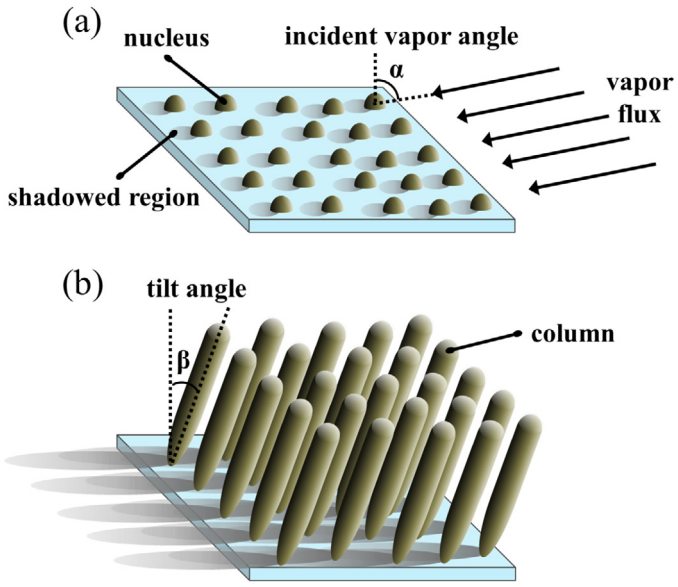

Fig. 2. Schematic illustrations exhibiting the growth mechanism of well-aligned slanted nanocolumnar structures during (a) the initial and (b) the subsequent stages of deposition.

tilted nanocolumnar structures, *i.e.*, arrays of slanted nanowires (Fig. 2). Herein, we demonstrate the fabrication of well-aligned slanted $LiCoO_2$ nanowires cathode-based all-solid-state thin film batteries, by the glancing angle deposition method. The resulting nanostructure was analyzed and the all-solid-state thin film battery was fabricated using well-aligned $LiCoO_2$ nanowires as a cathode, lithium phosphorus oxynitride (LiPON) as a solid electrolyte, and Li metal as an anode. We also compared the electrochemical performance of the 1D nanowire $LiCoO_2$ with that of the 2D planar $LiCoO_2$ thin film fabricated by the conventional PVD method. The rate capability performance of $LiCoO_2$ thin films with different morphologies were also characterized in terms of the electrochemical reaction kinetics at the interface between the solid electrolyte and the cathode.

2. Experimental procedure

2.1. Fabrication of the all-solid-state lithium ion battery with $LiCoO_2$ cathode

Prior to the deposition of $LiCoO_2$, a Pt film of 100 nm thickness as a current collector was deposited on a sapphire substrate (25 mm × 15 mm) by DC magnetron sputtering under Ar atmosphere at a gas flow rate of 50 sccm, and subsequently annealed at 700 °C for 1 h. The $LiCoO_2$ cathode thin film with an active area of 6 mm × 6 mm was deposited on the Pt-coated substrate at room temperature about 20 °C by RF magnetron sputtering with a $LiCoO_2$ target (LTS Research Laboratories, Inc., 2″) under a working pressure of 2.5 mTorr, and 100 W in Ar atmosphere. For the 1D $LiCoO_2$ nanowire cathode, during the deposition process, the substrate was placed at an angle of 50° with respect to the normal direction of the $LiCoO_2$ target surface, which can be defined as the incident vapor angle, α, for glancing angle deposition configuration (see Fig. 1b). While the 2D planar $LiCoO_2$ cathode was obtained at $\alpha = 0°$, which means that the target and the substrate surface are aligned in parallel, *i.e.*, conventional PVD method, as shown in Fig. 1a. After the deposition, both samples were annealed at 700 °C for 1 h in O_2 flow to enhance the crystallinity of the $LiCoO_2$ film. The weight of the $LiCoO_2$ active material was measured using an electronic micro balance (MSE3.6P-000-DM, Sartorius, Germany).

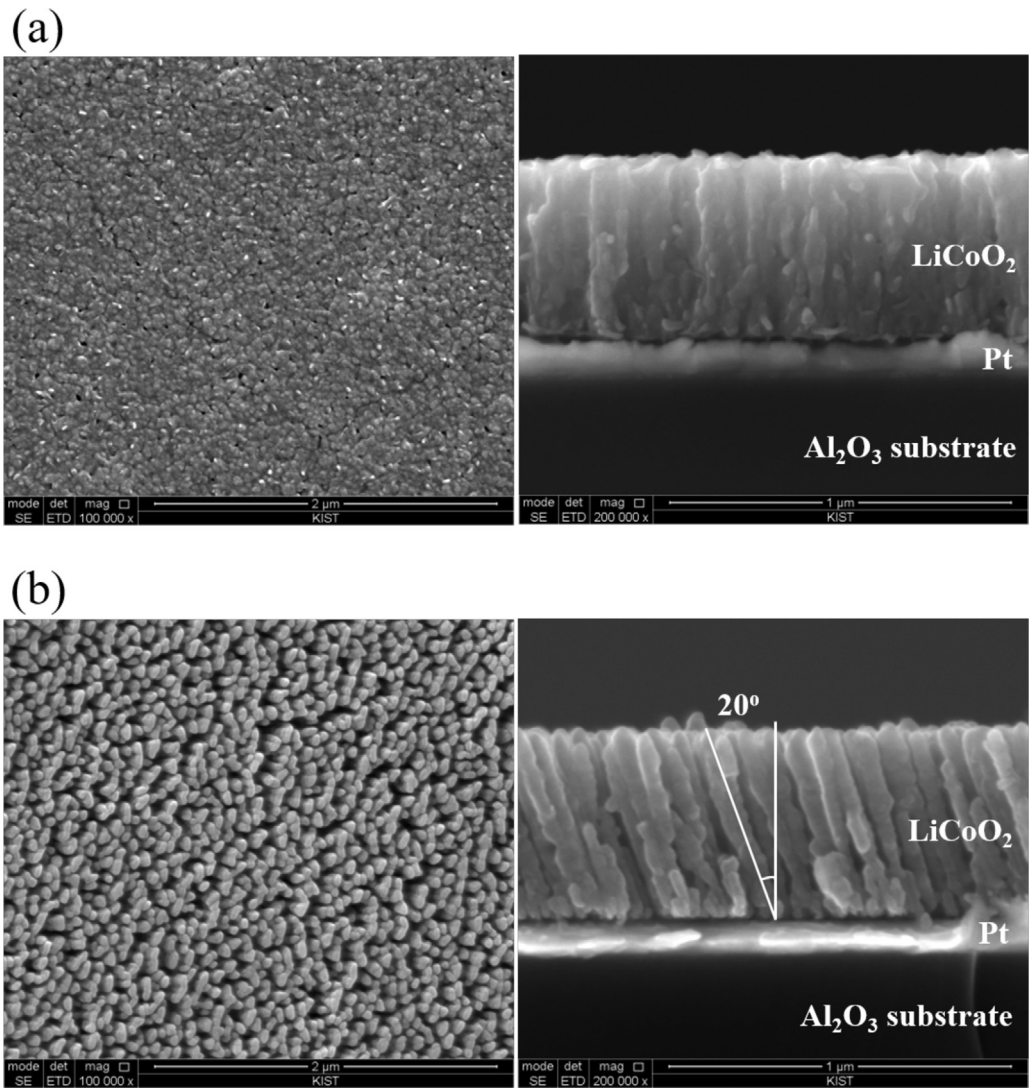

Fig. 3. SEM images of surface (left side) and cross-sectional (right side) views of the $LiCoO_2$ films fabricated by different deposition methods: (a) conventional PVD and (b) GLAD method.

2.2. Characterization

The surface morphology and thickness of the $LiCoO_2$ films were observed using scanning electron microscope (SEM, XL-30 E-SEM, FEI, Netherlands). Crystallographic information was obtained by X-ray diffraction (XRD, D/MAX-2500, Rigaku, Japan) with Cu-Kα radiation. To confirm the penetration depth of the solid electrolyte into the $LiCoO_2$ cathodes, elemental mapping was carried out using field emission electron microscope (FEM, JEM-2100F, JEOL, Japan) equipped with energy dispersive spectroscope (EDS). An electron-transparent specimen for the FEM images was prepared by focused ion beam (FIB, FIB-Quanta 3D, FEI, Netherlands) milling.

For electrochemical testing, a Ni current collector as a counter electrode was grown on the sapphire substrate by e-beam evaporation technique. Then, LiPON was deposited by reactive RF magnetron sputtering using a Li_3PO_4 target (DNT Korea Co., Ltd., 4″) at room temperature under a N_2 gas flow with working pressure of 5 mTorr. Finally, the counter electrode was deposited by thermal evaporation using Li metal in an Ar-filled glove box. The charge/discharge characteristics of the half-cell were evaluated using a battery test system (N174-HR, Toyo System Co., Ltd., Japan) over a potential range of 3.0–4.2 V at various current rates from 0.1–10 C at an interval of 5 cycles. Long-term cycling of the half-cell was carried out at a constant current rate of 1 C for 400 cycles. Electrochemical impedance spectroscopy (EIS, IM6ex Electrochemical Workstation, Zahner Elektrik GMBH & Co. KG, Germany) was also conducted in the frequency range of 1 MHz to 20 mHz with an amplitude of 10 mV.

3. Results and discussion

The $LiCoO_2$ film fabricated by the conventional PVD method (*i.e.*, sputtered at $\alpha = 0^\circ$) has an almost fully-dense microstructure with tightly-packed vertical columns, as shown in Fig. 3a, with a thickness of approximately 500 nm, while the $LiCoO_2$ sample fabricated by the GLAD method (*i.e.*, sputtered at $\alpha = 50^\circ$) exhibits a well-separated array of nanocolumns deposited on the Pt current collector (see Fig. 3b) in which areal density of the nanocolumns was estimated to be $1.46 \times 10^{10}\ cm^{-2}$ from image analysis. The cross-sectional view of the sample fabricated by the GLAD method clearly shows the nanocolumnar structured slanted $LiCoO_2$ nanowires that are formed due to the shadowing effect [19–22]. Each nanowire has an average diameter and length of 58 ± 1 and 557 ± 3 nm, respectively. The tilt angle β (see Fig. 1b) between the nanowire columns and the normal to the substrate is determined by the angle (α) of incident vapor flux (50°). Gener-

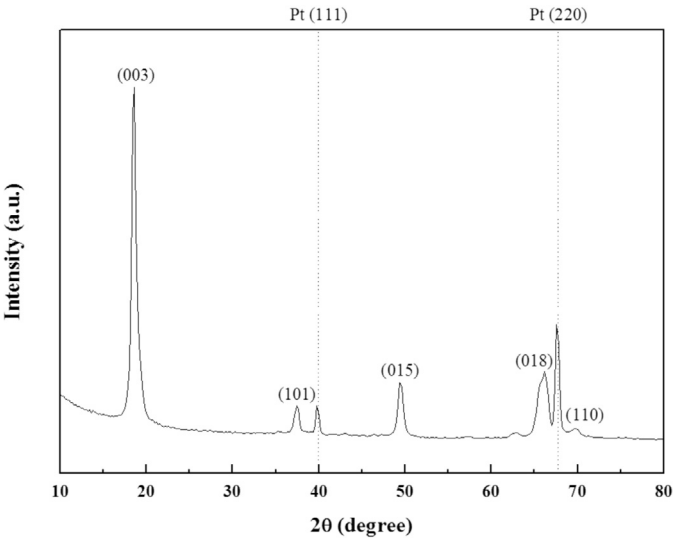

Fig. 4. XRD pattern of the well-aligned $LiCoO_2$ nanowires deposited on the Pt current collector.

ally, β is smaller than α, following the empirical expressions for the GLAD method: the tangent rule ($\tan\alpha = 2\tan\beta$ when $\alpha \leq 60^\circ$) or the cosine rule ($\beta = \alpha - \text{arc sin}\,[(1-\cos\alpha)/2]$ when $\alpha > 60^\circ$) [22–24]. In our study, β was calculated as 31° using the tangent rule. However, the measured value of β was ~20° (Fig. 3b), 11° lesser than the calculated value. In the sputtering system, the particles released from the target collide with the gas molecules, *i.e.*, plasma ions, which are present between the target and the substrate, which likely deviates the trajectory of the flying particles [25,26]. Consequently, the actual angle of incoming particles toward the substrate would be different from α, resulting in this discrepancy. Overall, the $LiCoO_2$ thin film composed of well-aligned inclined nanowires has a thickness of ~500 nm, with many empty interspaces between the nanowires, which not only facilitates the penetration of the solid electrolyte phase into the cathode for intimate contact, but also alleviates the volumetric variation-induced stress that occurs upon cycling.

The XRD pattern for the $LiCoO_2$ nanowires is shown in Fig. 4. There exists a very strong peak at 18.6° corresponding to the (003) diffraction of crystalline $LiCoO_2$ (JCPDS 44-0145), while other small peaks at 37.4°, 49.4°, and 66.2° are attributed to the (101), (015), and (018) diffraction peaks, respectively. The $LiCoO_2$ nanowires obtained from GLAD method were found to exhibit a preferred orientation of (003). Since the layered-hexagonal nature of $LiCoO_2$ determines the direction of facile ion flow, which follows a normal direction to the basal plane of (001) [4,6,27], the lithium ions would suffer from sluggish diffusion in a perpendicular direction to the $LiCoO_2$ crystal plane when (003) is the preferred orientation. This likely becomes worse in a dense $LiCoO_2$ film with (003) preferred orientation, impeding the reaction kinetics of lithium ions and in turn the performance of the all-solid-state thin film batteries. By contrast, our well-aligned slanted $LiCoO_2$ nanowires readily permit the penetration of solid electrolyte particles of LiPON into the empty interspaces between the slanted $LiCoO_2$ nanowires. This allows contact formation between the solid electrolyte and the cathode, not only at the top surfaces, but also at the lateral surfaces of the $LiCoO_2$ nanowires. Therefore, despite the (003) oriented $LiCoO_2$ nanowires, it is expected that the electrochemical kinetics at the solid electrolyte/cathode interface improves due to the enlarged reaction sites.

In order to verify the phase distribution of the LiPON solid electrolyte into the $LiCoO_2$ cathodes, EDS elemental mapping was performed as shown in Fig. 5a–f. Detection of Co and P indicates the presence of $LiCoO_2$ and LiPON phases, respectively. In the dense $LiCoO_2$ thin film (Fig. 5a–c), the spatial distributions of Co and P elements were clearly distinguished along the boundary region between the $LiCoO_2$ cathode and LiPON solid electrolyte, whereas the well-aligned slanted $LiCoO_2$ nanowires showed an obviously different result (Fig. 5d–f). It was clearly observed that the solid electrolyte phase covers both the top surfaces and lateral surfaces of the $LiCoO_2$ nanowires and the penetration depth of LiPON is ~110 nm. In order to elucidate the improvement in the contact area between the solid electrolyte and the cathode, two different thin film $LiCoO_2$ cathodes with either dense planar structure or nanowire arrays were investigated. As shown in Fig. 5g, the dense $LiCoO_2$ thin film has a 2D planar interface with the LiPON solid electrolyte, and the contact area can thus be recognized as the active reaction area of 0.36 cm^2. Based on the observed nanowire morphology, a schematic cross-sectional microstructure for the slanted $LiCoO_2$ nanowires in contact with LiPON is depicted in Fig. 5h. The contact area of each slanted nanowire is represented by an oblique cylinder with (1) hemispherical cap with the diameter of ~58 nm, (2) cylinder with a height of 71 nm, and (3) slanted cut cylinder with the height of 21 nm (Fig. 5i). The number of nanowires presented in the cathode active area of 0.36 cm^2 is $\sim 5.4 \times 10^9$. Thus, the estimated contact area of the well-aligned $LiCoO_2$ nanowires is ~1.08 cm^2, which is three times as high as that of the dense $LiCoO_2$ thin film. Thus, the GLAD method effectively increases the contact area between the LiPON solid electrolyte and the slanted $LiCoO_2$ nanowire cathode. Furthermore, the lateral surfaces of the $LiCoO_2$ nanowires, which are normal to the basal plane, are exposed to the solid state electrolyte for better lithium ion diffusion.

Fig. 6a exhibits the first discharge profiles of the well-aligned slanted $LiCoO_2$ nanowires under different current rates from 0.1–10 C in the voltage range 3.0–4.2 V. To show the electrochemical performance of thin film lithium ion batteries, the volumetric capacity is generally used with the assumption that the cathode thin film has a dense rectangular shape. However, our sample involved highly porous thin films, so the unit of specific capacity was used. The nanowire-structured $LiCoO_2$ thin film cathode showed a typical voltage plateau around 3.9 V, indicative of the Co^{3+}/Co^{4+} redox couple. Specific discharge capacities at 0.1, 0.2, 0.5, 1, 2, 5, and 10 C are 97.3, 93.1, 88.7, 85.2, 81.0, 72.4, and 57.5 mAh g^{-1}, respectively. The rate capability of the well-aligned slanted $LiCoO_2$ nanowires was compared with those of the dense $LiCoO_2$ thin films previously reported in literature [8] and prepared by our group using conventional PVD method. As shown in Fig. 6b, the capacity values as a function of different current rates were normalized by the values measured at 0.1 C. The normalized discharge capacities of both the slanted nanowire $LiCoO_2$ thin film and the dense $LiCoO_2$ thin films decreased upon increasing the current rate. It is anticipated that the nanowires cell would have a better rate capability than the dense $LiCoO_2$ thin film because the estimated contact area of our sample is three times wider than the dense $LiCoO_2$ thin film, giving the higher areal density of electrochemically active sites. The nanowires cell manifests the superior rate capability at all current rates as compared to those of our thin film cell as expected. On the other hand, the normalized specific capacities of the nanowires based cell below charging/discharging rates of 2 C are similar, or slightly smaller as compared to those of a previous work using $LiCoO_2$ thin film. The similar or slightly lower rate capability at moderately low current rates could be attributed to the following conjectures; (i) facile formation of solid electrolyte interphase (SEI) layers in the nanowire-structured $LiCoO_2$ is highly probable owing to the much higher specific surface area of the nanowires and (ii) the charge transfer reaction does not prevail the overall reaction kinetics of the electrochemical reaction at relatively low current rates. These constraints are plausible considering the facts that the enlarged interfacial area of the nanowires cell

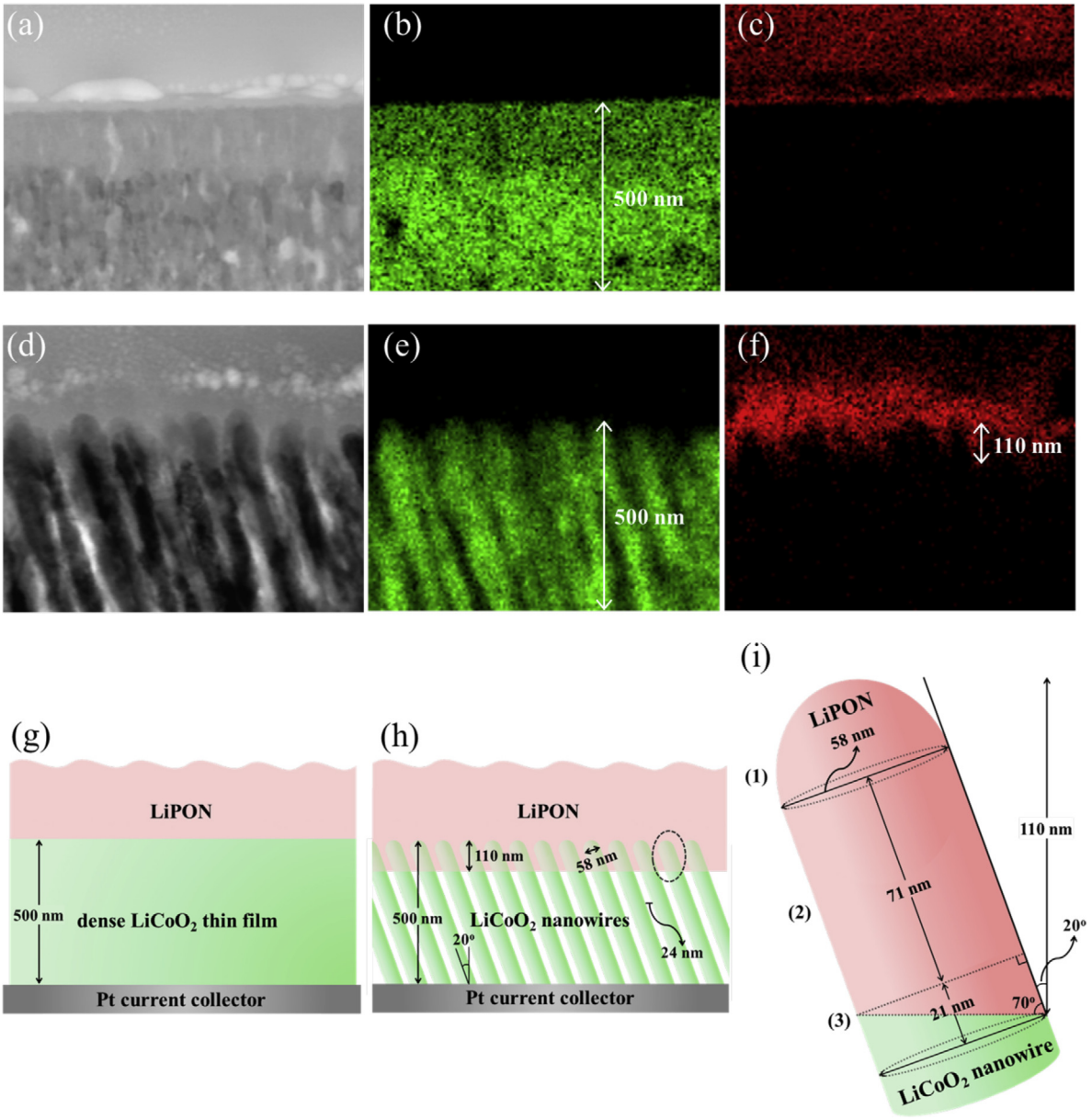

Fig. 5. EDS elemental mapping images of the LiPON-deposited dense $LiCoO_2$ thin film and well-aligned $LiCoO_2$ slanted nanowires: (a) and (d) cross sectional FEM images, (b) and (e) distribution mappings of Co, and (c) and (f) distribution mappings of P. Schematics showing the cross sections of the LiPON-deposited $LiCoO_2$ cathodes with two different electrode morphologies: (g) dense thin film cathode and (h) slanted nanowires cathode. (i) Enlarged the LiPON-deposited slanted nanowire cathode.

and similar high and low frequency polarization resistances (in the same order) are observed. The follow-up studies for the elucidation of detailed reaction kinetics will be conducted in the near future. However, the normalized capacity of the dense $LiCoO_2$ thin film suddenly dropped at a high current rate above 3 C, and at 5 C the sample showed a poor discharge capacity of 39% with respect to the capacity measured at 0.1 C. On the other hand, the discharge capacities of the slanted $LiCoO_2$ nanowires at 5 and 10 C were 75% and 60%, respectively. In all-solid-state thin film batteries, a high current rate means that a significant amount of lithium ions should simultaneously pass through the thin films. Thus, the electrochemical reaction kinetics at the solid electrolyte/solid electrode interface would determine the cell performance. In the case of the $LiCoO_2$ nanowires, the increased contact area between the LiPON solid electrolyte/electrode interface can provide additional migration pathways for lithium ion diffusion, resulting in enhanced electrochemical kinetics, and thereby yielding better rate capability than the dense $LiCoO_2$ thin film. On the other hand, the Coulombic efficiencies (CEs) of the dense $LiCoO_2$ thin film and well-aligned $LiCoO_2$ nanowires exhibit nearly 100% at all current rates of 0.1–10 C, as shown in Fig. 6b (dotted lines).

The cyclability of the well-aligned slanted $LiCoO_2$ nanowires is depicted in Fig. 7a, where the current rates are gradually increased from 0.1 to 10 C and then returned back to 0.1 C. At the initial condition of 0.1 C, the nanowire $LiCoO_2$ cathode thin film exhibited a high specific discharge capacity of 97.3 mAh g^{-1}, which indicates a high practical performance of 71.1% with respect to the theoretical specific capacity of 136.9 mAh g^{-1}. The $LiCoO_2$ nanowires showed a moderate specific discharge capacity up to 2 C and then delivered specific discharge capacities of 71.9 mAh g^{-1} and 59.4 mAh g^{-1} even at high current rates of 5 and 10 C, respectively. At the final condition of 0.1 C, the sample showed high capacity retention of 92%, suggesting that the nanowire-structured $LiCoO_2$ cathode

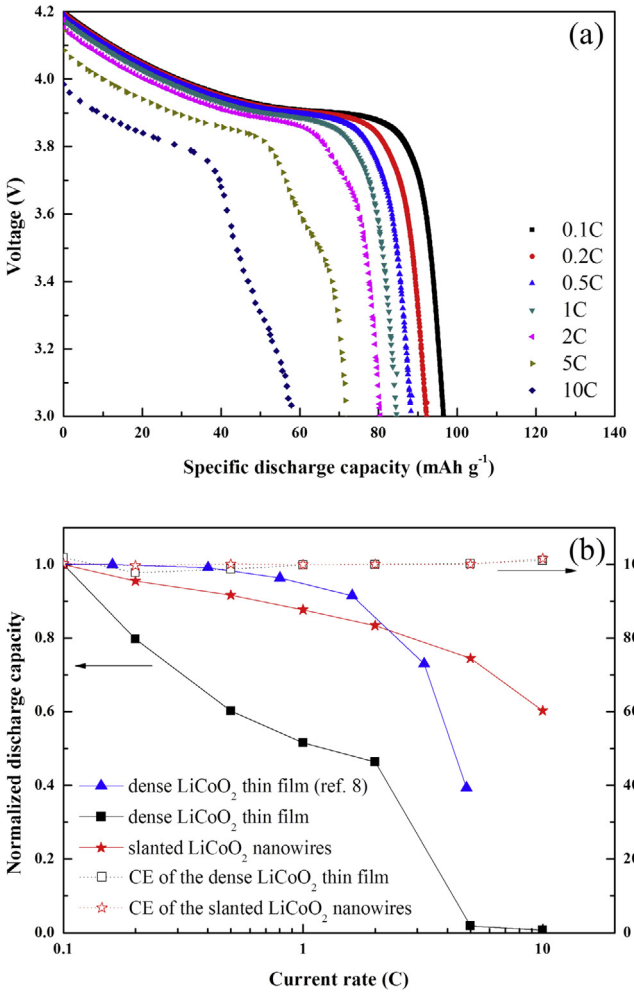

Fig. 6. (a) Discharge profiles of the well-aligned $LiCoO_2$ slanted nanowires with various current rates from 0.1 C to 10 C. (b) Relative rate capability normalized by the capacity value at 0.1 C for comparing the $LiCoO_2$ slanted nanowires with the dense $LiCoO_2$ thin films and Coulombic efficiency *vs.* a current rate of 0.1–10 C for the dense $LiCoO_2$ thin film and the well-aligned $LiCoO_2$ slanted nanowires.

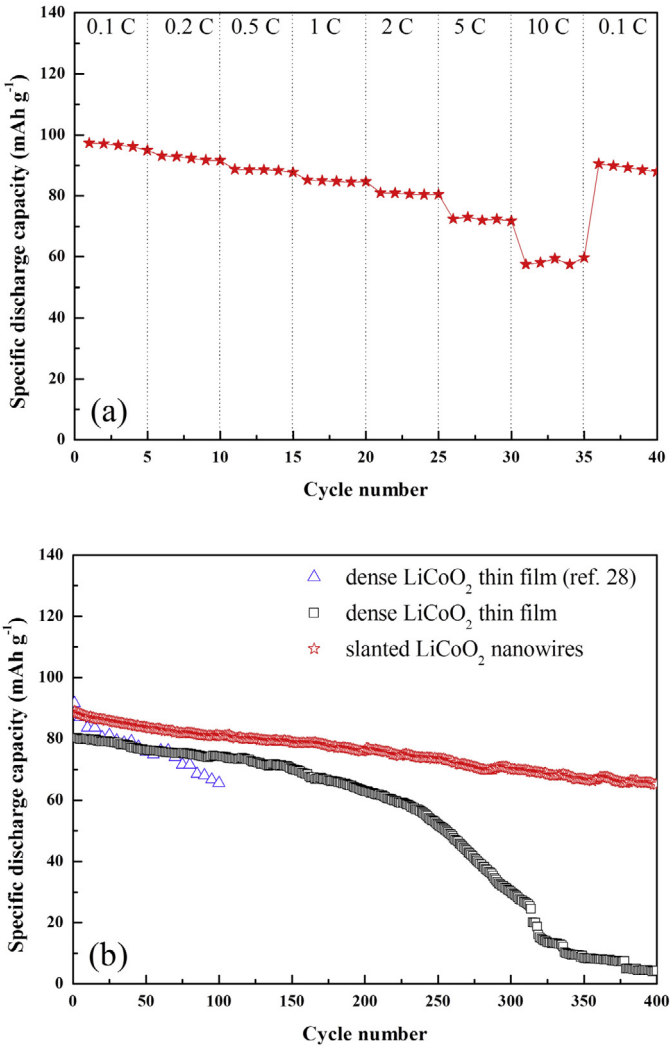

Fig. 7. (a) Cyclability of the well-aligned $LiCoO_2$ slanted nanowires with various current rates from 0.1 C to 10 C. (b) Specific discharge capacity *vs.* cycle number for the $LiCoO_2$ cathodes with two different morphologies at the current rate of 1 C.

thin film has low irreversible degradation during repeated lithiation/delithiation under various current rates.

Fig. 7b shows the long-term cycling stability of the cells based on the dense $LiCoO_2$ thin film and the well-aligned slanted $LiCoO_2$ nanowires, in which the cycling behavior of a previously reported literature is plotted together for comparison [28]. All capacity values are collected during the cycling at 1 C. Our $LiCoO_2$ based cells exhibit superior cycling stability than the previously reported one regardless of microstructure of $LiCoO_2$. After 100 cycles, the previously reported thin film cell represents the capacity retention of 72% of the one at the first cycle, which was attributed to thermally induced defects such as micro-cracks at the $LiCoO_2$ cathode during the post-annealing process [28]. On the other hand, the nanowire and thin film cells in this work shows the similar capacity retentions of 89% and 88%, respectively, with an irreversible capacity loss of 0.08% per cycle after 150 cycles of charging/discharging. The nanowire cell maintains its cycling stability up to 400 cycles with similar degradation rate, whereas the capacity decrease rate of the thin film cell gradually increases after 150 cycles, in turn, the capacity is totally deteriorated to 5% of capacity retention after 400 cycles. The inferior long-term cycling stability of the thin film cell can be attributed to insufficient damage tolerance to accommodate mechanical stresses during cycling, followed by the formation of defects such as micro-cracks at the $LiCoO_2$ cathode. This cycling instability can be circumvented by nanostructuring of $LiCoO_2$ cathode, which may be due to the robustness of LiPON/$LiCoO_2$ interface by three-dimensional integration. In the well-aligned $LiCoO_2$ nanowires, the thermally and mechanically induced stresses during post-annealing and electrochemical cycling were alleviated due to the well-separated slanted nanowire structures. This unique nanostructure can act as a "stress reliever", enabling the enhanced cycling performance [15]. Consequentially, after 400 cycles, the well-aligned slanted $LiCoO_2$ nanowires showed high long-term stability with high capacity retention of 73%.

The EIS responses of $LiCoO_2$ electrodes in a half cell configuration consist of mainly three different polarizations: (i) polarization due to the conduction of Li^+ ions through solid electrolyte at high frequency (~10 kHz) (ii) interfacial polarization of the Li/solid electrolyte interface at mid frequency (~1 kHz) (iii) charge transfer polarization of $LiCoO_2$ at low frequency (<100 Hz) [29,30]. In general, the interfacial polarization of the Li/solid electrolyte is much smaller than the other polarizations, which gives rise to the manifestation of two distinct semicircles, rather than three [30]. Similar to the previous works, Nyquist plots of the dense $LiCoO_2$ thin film and the well-aligned $LiCoO_2$ slanted nanowires exhibit two clear semicircles with Warburg-type blocking behaviors owing to the Li ion blocking at $LiCoO_2$ electrodes as shown in Fig. 8. Note that all EIS

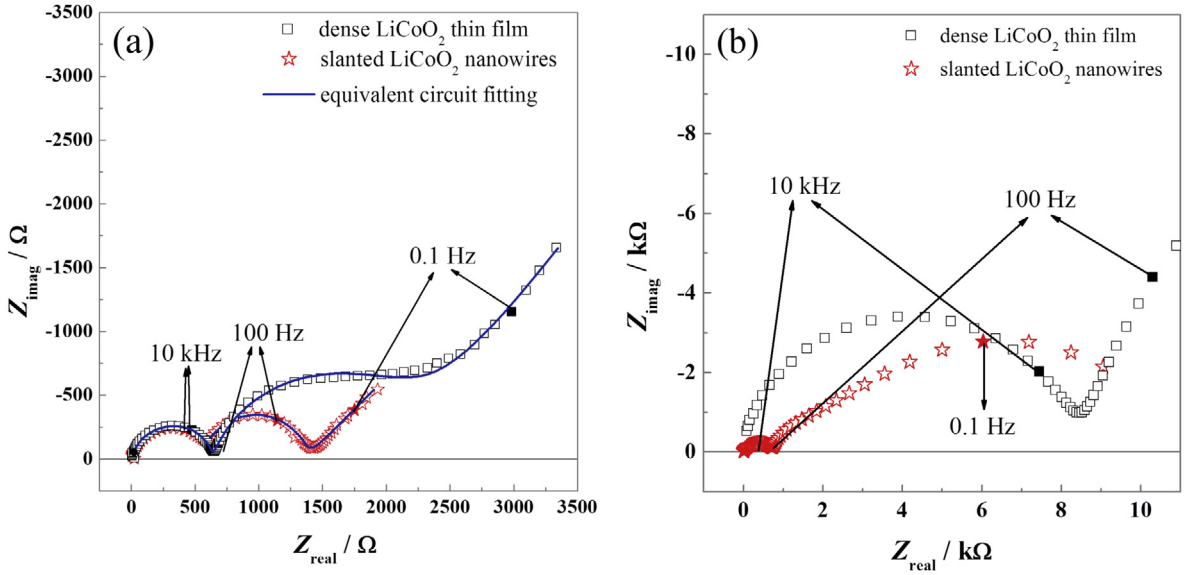

Fig. 8. Nyquist plots of the dense $LiCoO_2$ thin film and the well-aligned $LiCoO_2$ slanted nanowires based cells. (a) Nyquist plots of the cells discharged to 3.0 V *vs.* Li/Li^+ from as-fabricated states. (b) Nyquist plots of the cells after 400 times of cycling.

measurements were conducted with fully lithiated $LiCoO_2$ at 3.0 V. The equivalent circuit fittings based on the polarization processes described above fit well to the measured spectra as depicted in Fig. 8a (blue lines). The polarization resistances for the conduction through LiPON electrolyte are similar for both samples considering the fitting error of 12.4%, which are 479 and 530 Ω for the nanowires and thin film based cells, respectively. This observation clearly shows that the ionic conductivity of LiPON layer for both cells is nearly identical regardless of their electrode structure. On the other hand, the charge transfer polarization resistance of the nanowires based cell is much smaller than that of the thin film cell. The polarization resistance of the nanowires cell is 786 Ω, while that of the thin film cell is 1689 Ω. The superior charge transfer kinetics of the nanowires cell, *i.e.*, much smaller charge transfer polarization, can be conceived as the accelerated reaction kinetics of the $LiCoO_2$ nanowires assembly, which can be ascribed to the increased electrochemically active sites upon the percolation of LiPON phase into spacing between $LiCoO_2$ nanowires.

After the 400 cycling in the voltage range of 3.0–4.2 V *vs.* Li/Li^+, EIS responses of the nanowires and thin film cells vary dramatically as presented in Fig. 8b. The high frequency polarizations by Li^+ conductions through LiPON increase to 700 and 8800 Ω for the nanowires and thin film cells, respectively. The relatively small increase in the high frequency polarization of the nanowires cell implies that the ionic conduction pathway of the nanowires cell is preserved under the strain exerted by repeated cycling, which may be attributed to the three-dimensionally connected LiPON and $LiCoO_2$ by nanostructuring. Two-dimensionally connected LiPON and $LiCoO_2$ thin films cannot endure the stress during cycling as reflected by the huge increase in the high frequency polarization by a factor of 16.6. On the other hand, the charge transfer polarization at low frequency of the nanowires cell is augmented to ~9400 Ω, which shows the disruption of LiPON/$LiCoO_2$ interface. Because the increase of the polarization resistance for ionic conduction is not significant, the increase in the charge transfer polarization may be impeded either by the disrupted LiPON/$LiCoO_2$ interface or the evolution of the SEI. The charge transfer polarization of the thin film electrode manifests the catastrophic failure of the cell, of which the low frequency polarization is above 80 kΩ. In these regards, it can be concluded that the $LiCoO_2$ nanowires based cell effectively improves the charge transfer kinetics because of higher active reaction site and the long-term stability owing to its three-dimensionally connected interface structure.

4. Conclusions

We successfully fabricated well-aligned slanted $LiCoO_2$ nanowires as a one-dimensional nanostructured cathode by glancing angle deposition to enhance the electrochemical performance of all-solid-state thin film batteries. The well-separated slanted $LiCoO_2$ nanowires with empty interspaces between the nanowires not only facilitates the penetration of the solid electrolyte phase of LiPON into the $LiCoO_2$ cathode, but also alleviated thermally and mechanically induced stresses during post-annealing and electrochemical cycling. Despite the (003) oriented $LiCoO_2$ nanowires, our slanted $LiCoO_2$ nanowires showed high discharge capacities of 75% and 60% at high current rates of 5 C and 10 C, respectively, with respect to the initial capacity measured at 0.1 C, owing to the enlarged contact area between the LiPON solid electrolyte/$LiCoO_2$ cathode. Moreover, after 400 cycles, the slanted $LiCoO_2$ nanowires still retained a high capacity of 73%, due to their "stress reliever" properties, arising from their well-separated slanted nanowire structure. The electrochemical performance of the all-solid-state thin film battery involving the well-aligned slanted $LiCoO_2$ nanowires is significantly enhanced in terms of the rate capability and long-term cycling stability when compared to the conventional dense $LiCoO_2$ thin films.

Acknowledgements

This work was supported by a National Research Foundation of Korea (NRF) grant funded by the Korean government (MSIP) (Nos. 2010-00289754 and 2012R1A3A2026417). We thank Dr. Heesoo Kim for conducting FIB and SEM analyses.

References

[1] M. Ollinger, H. Kim, T. Sutto, A. Piqué, Laser printing of nanocomposite solid-state electrolyte membranes for Li micro-batteries, Appl. Surf. Sci. 252 (2006) 8212–8216.
[2] D.C. Bock, A.C. Marschilok, K.J. Takeuchi, E.S. Takeuchi, Batteries used to power implantable biomedical devices, Electrochim. Acta 84 (2012) 155–164.

[3] Y. Wang, B. Liu, Q. Li, S. Cartmell, S. Ferrara, Z.D. Deng, J. Xiao, Lithium and lithium ion batteries for applications in microelectronic devices: a review, J. Power Sources 286 (2015) 330–345.
[4] Y.-N. Zhou, M.-Z. Xue, Z.-W. Fu, Nanostructured thin film electrodes for lithium storage and all-solid-state thin-film lithium batteries, J. Power Sources 234 (2013) 310–332.
[5] K. Takada, Progress and prospective of solid-state lithium batteries, Acta Mater. 61 (2013) 759–770.
[6] Y. Yoon, C. Park, J. Kim, D. Shin, Lattice orientation control of lithium cobalt oxide cathode film for all-solid-state thin film batteries, J. Power Sources 226 (2013) 186–190.
[7] N.J. Dudney, Y.-I. Jang, Analysis of thin-film lithium batteries with cathodes of 50 nm to 4 μm thick $LiCoO_2$, J. Power Sources 119–121 (2003) 300–304.
[8] B. Wang, J.B. Bates, F.X. Hart, B.C. Sales, R.A. Zuhr, J.D. Robertson, Characterization of thin-film rechargeable lithium batteries with lithium cobalt oxide cathodes, J. Electrochem. Soc. 143 (1996) 3203–3213.
[9] N. Kamaya, K. Homma, Y. Yamakawa, M. Hirayama, R. Kanno, M. Yonemura, T. Kamiyama, Y. Kato, S. Hama, K. Kawamoto, A. Mitsui, A lithium superionic conductor, Nat. Mater. 10 (2011) 682–686.
[10] G. Oh, M. Hirayama, O. Kwon, K. Suzuki, R. Kanno, Bulk-type all solid-state batteries with 5 V class $LiNi_{0.5}Mn_{1.5}O_4$ cathode and $Li_{10}GeP_2S_{12}$ solid electrolyte, Chem. Mater. 28 (2016) 2634–2640.
[11] Z. Liu, W. Fu, E.A. Payzant, X. Yu, Z. Wu, N.J. Dudney, J. Kiggans, K. Hong, A.J. Rondinone, C. Liang, Anomalous high ionic conductivity of nanoporous β-Li_3PS_4, J. Am. Chem. Soc. 135 (2013) 975–978.
[12] G. Sahu, Z. Lin, J. Li, Z. Liu, N. Dudney, C. Liang, Air-stable, high-conduction solid electrolytes of arsenic-substituted Li_4SnS_4, Energy Environ. Sci. 7 (2014) 1053–1058.
[13] J. Li, C. Ma, M. Chi, C. Liang, N.J. Dudney, Solid electrolyte: the key for high-voltage lithium batteries, Adv. Energy Mater. 5 (2015) 1401408.
[14] J.B. Goodenough, P. Singh, Review – solid electrolytes in rechargeable electrochemical cells, J. Electrochem. Soc. 162 (2015) A2387–A2392.
[15] B.D. Polat, O. Keles, K. Amine, Silicon–copper helical arrays for new generation lithium ion batteries, Nano Lett. 15 (2015) 6702–6708.
[16] Y. Zhou, C. Shen, H. Li, Synthesis of high-ordered $LiCoO_2$ nanowire arrays by AAO template, Solid State Ionics 146 (2002) 81–86.
[17] C.L. Liao, M.T. Wu, J.H. Yen, I.C. Leu, K.Z. Fung, Preparation of RF-sputtered lithium cobalt oxide nanorods by using porous anodic alumina (PAA) template, J. Alloys Compd. 414 (2006) 302–309.
[18] H. Xia, Y. Wan, W. Assenmacher, W. Mader, G. Yuan, L. Lu, Facile synthesis of chain-like $LiCoO_2$ nanowire arrays as three-dimensional cathode for microbatteries, NPG Asia Mater. 6 (2014) e126.
[19] M.M. Hawkeye, M.J. Brett, Glancing angle deposition: fabrication, properties, and applications of micro- and nanostructured thin films, J. Vac. Sci. Technol. A 25 (5) (2007) 1317–1335.
[20] S.M. Haque, K.D. Rao, J.S. Misal, R.B. Tokas, D.D. Shinde, J.V. Ramana, S. Rai, N.K. Sahoo, Study of hafnium oxide thin films deposited by RF magnetron sputtering under glancing angle deposition at varying target to substrate distance, Appl. Surf. Sci. 353 (2015) 459–468.
[21] M.O. Jensen, M.J. Brett, Periodically structured glancing angle deposition thin film, IEEE Trans. Nanotechnol. 4 (2005) 269–277.
[22] A. Barranco, A. Borras, A.R. Gonzalez-Elipe, A. Palmero, Perspectives on oblique angle deposition of thin films from fundamentals to devices, Prog. Mater. Sci. 76 (2016) 59–153.
[23] J.M. Nieuwenhuizen, H.B. Haanstra, Microfractography of thin films, Philips Tech. Rev. 27 (1966) 87–91.
[24] R.N. Tait, T. Smy, M.J. Brett, Modelling and characterization of columnar growth in evaporated films, Thin Solid Films 226 (1993) 196–201.
[25] P. Pedrosa, C. Lopes, N. Martin, C. Fonseca, F. Vaz, Electrical characterization of Ag:TiN thin films produced by glancing angle deposition, Mater. Lett. 115 (2014) 136–139.
[26] L. Qiao, P. Wang, L. Chai, X. Zhang, W. Liu, Influence of the incident flux angles on the structures and properties of magnetron sputtered MoS_2 films, J. Phys. D: Appl. Phys. 48 (2015) 175304.
[27] J.B. Bates, N.J. Dudney, B.J. Neudecker, F.X. Hart, H.P. Jun, S.A. Hackney, Preferred orientation of polycrystalline $LiCoO_2$ films, J. Electrochem. Soc. 147 (1) (2000) 59–70.
[28] H.Y. Park, S.R. Lee, Y.J. Lee, B.W. Cho, W.I. Cho, Bias sputtering and characterization of $LiCoO_2$ thin film cathodes for thin film microbattery, Mater. Chem. Phys. 93 (2005) 70–78.
[29] S. Laraillou, D. Guy-Bouyssou, F. le Cras, S. Franger, Comprehensive characterization of all-solid-state thin films commercial microbatteries by electrochemical impedance spectroscopy, J. Power Sources 319 (2016) 139–146.
[30] Y. Iriyama, T. Kako, C. Yada, T. Abe, Z. Ogumi, Charge transfer reaction at the lithium phosphorus oxynitride glass electrolyte/lithium cobalt oxide thin film interface, Solid State Ionics 176 (2005) 2371–2376.